IEEE Photonics Journal
An IEEE Photonics Society Publication

Open Access

Spectral Polarization Spreading Behaviors in Stimulated Brillouin Scattering of Fibers

Volume 9, Number 1, February 2017

Chunhua Wang
Qiwen Zhang
Chengbo Mou
Liang Chen
Xiaoyi Bao

$$\frac{d\hat{s}}{dz} = \vec{\beta}_s \times \hat{s} + \frac{r_0 I_p}{1+\xi^2}\left[\hat{p} - (\hat{s}\cdot\hat{p})\hat{s}\right] + \frac{r_0 \xi}{1+\xi^2} I_p (\hat{s}\times\hat{p})$$

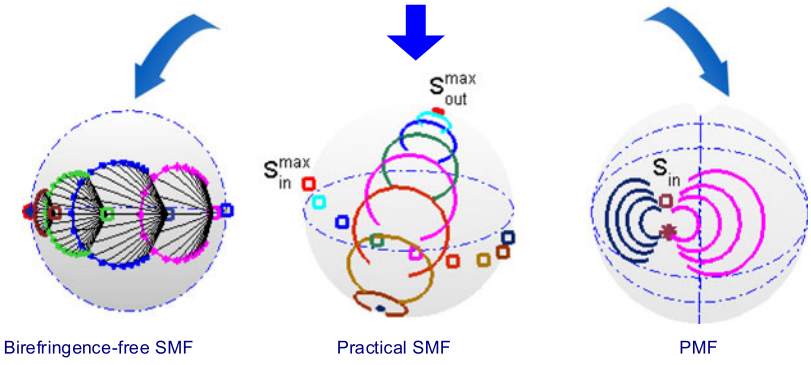

DOI: 10.1109/JPHOT.2017.2653858
1943-0655

IEEE photonics SOCIETY

IEEE

Spectral Polarization Spreading Behaviors in Stimulated Brillouin Scattering of Fibers

Chunhua Wang,[1] Qiwen Zhang,[1] Chengbo Mou,[1] Liang Chen,[2] and Xiaoyi Bao[2]

[1]Laboratory of Specialty Fiber and Broadband Access Network, Shanghai University, Shanghai 200444, China
[2]Fiber Optics Group, Department of Physics, University of Ottawa, Ottawa, ON K1N 6N5, Canada

DOI:10.1109/JPHOT.2017.2653858

Manuscript received November 9, 2016; revised December 26, 2016; accepted January 11, 2017. Date of publication January 17, 2017; date of current version February 8, 2017. The work was supported in part by the National Natural Science Foundations of China under Grant 61575118/61077018/61635006, in part by Shanghai Leading Academic Discipline under Project SKLFSO2012-06, and in part by the Scholarship from Shanghai Municipal Education Commission. Corresponding author: C. Wang (e-mail: lizawch@staff.shu.edu.cn).

Abstract: A vector theoretical model involving the polarization spectrum behavior of the stimulated Brillouin scattering (SBS) is proposed. It reveals a phenomenon of spectral polarization spreading, i.e., the states of polarization of different frequency components of signal light experience distinct SBS pulling. The polarization behaviors in birefringence-free single-mode fiber (SMF), practical SMF, and polarization maintaining fiber (PMF) are investigated by analytical discussion, simulation, and experiment. It is found that in arbitrary fiber, the concurrent polarization evolution induced by fiber birefringence and SBS polarization spreading can be decomposed as a linear fiber birefringence rotation, followed by the SBS polarization spreading effect. The orientation and the size of SBS polarization spreading in the free-depletion regime are explicitly determined. Moreover, an orientation switching performance of the polarization spreading is observed in PMF. Finally, we demonstrate the SBS polarization spreading in SMF and PMF experimentally, and good agreement with theory is found.

Index Terms: Stimulated Brillouin scattering, birefringence, polarization, nonlinear optics, fibers.

1. Introduction

Stimulated Brillouin scattering (SBS) has found various applications in fiber lasers, long distance sensing, optical buffing, etc. [1]–[3]. As other optical nonlinearities could induce polarization transform, SBS is also able to induce nonlinear polarization evolution, called SBS pulling, from which potential applications can be raised, such as polarization controlling [4], fiber birefringence estimation [5]. Zadok *et al.* firstly reported the SBS polarization pulling [6] and studied its effect on the SBS gain in birefringent fiber through a vector theoretical model [7]. It is found that arbitrary states of polarization (SOPs) of signal light are always pulled towards the same target SOP point by SBS pulling. The target SOP point is the output SOP of the signal light which experiences the maximum SBS gain [6]. In addition, Fatome *et al.* reported another SBS polarization wheeling phenomenon in polarization maintaining fibers (PMFs) [8]. It is found that the output SOPs of signals with arbitrary

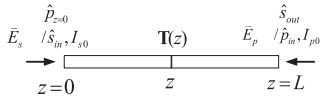

Fig. 1. SBS interaction diagram.

input SOPs will be concentrated to the $s_1 = 0$ circle on the Poincaré sphere when SBS works in heavy-depletion situations. However, all previous studies on SBS pulling are about the central wavelength of SBS gain spectrum, no study on the spectral SBS polarization behavior has been reported yet. In this paper, we extend the vector model of [6] from the central frequency to the spectrum scope, and find that different frequency components of signal light experience distinct SBS pullings, resulting in a spectral polarization spreading phenomenon in SBS. In this paper, the SBS spreading evolutions in birefringence-free single mode fiber (SMF), practical SMF with random birefringence, and PMF are analytically discussed and simulated. The explicit formula to quantify the spreading size in depletion-free regime is derived by sloving vector equation in birefringence-free fiber and adopting a matrix model in practical fiber. At the end of the paper, the SBS polarization spreadings in an SMF and a PMF are demonstrated experimentally.

2. Principle of SBS Polarization Spreading

When a signal light $\vec{E}_s$ is launched into an SMF with length L from $z = 0$, and a pump light $\vec{E}_p$ from $z = L$, as shown in Fig. 1, SBS occurs only if the pump power exceeds the SBS threshold. Under the stationary condition for CW lights, the SBS interaction among the signal, pump, and the acoustic wave ρ in lossless fibers is described by the following field propagation equations [6], [9], [10]:

$$\begin{aligned}
\frac{d\vec{E}_p}{dz} &= \frac{d\mathbf{T}^*(z)}{dz}\mathbf{T}^T(z)\vec{E}_p + j\frac{\omega_p \gamma_e}{2nc\rho_0}\rho\vec{E}_s \\
\frac{d\vec{E}_s}{dz} &= \frac{d\mathbf{T}(z)}{dz}\mathbf{T}^\dagger(z)\vec{E}_s + j\frac{\omega_s \gamma_e}{2nc\rho_0}\rho^*\vec{E}_p \\
\rho &= \frac{\varepsilon_0 \gamma_e q^2}{4\pi^2(v_B^2 - v^2 - jv\Gamma_B)}\vec{E}_s^\dagger\vec{E}_p
\end{aligned} \tag{1}$$

wherein **T**(z) denotes the Jones matrix of the fiber segment from $z = 0$ to z. The superscripts "*," "T," and "†" refer to conjugation, transpose, and transpose conjugation, respectively. $\omega_{p,s}$ is the angle frequency of pump or signal, c the light velocity in vacuum, n the average index of fiber, ε_0 the vacuum dielectric constant, γ_e the electrostrictive coefficient, ρ_0 the fiber density, q the acoustic wave vector, Γ_B the full width at half maximum (FWHM) of SBS gain, and v_B the Brillouin frequency shift (BFS).

By the relations of power, Stokes vectors of signal and pump lights to their fields: $I_{s,p} = 2n\varepsilon_0 c\vec{E}_{s,p}^\dagger\vec{E}_{s,p}$, $\hat{s} = (\vec{E}_s^\dagger\vec{\sigma}\vec{E}_s)/(\vec{E}_s^\dagger\vec{E}_s)$, and $\hat{p} = (\vec{E}_p^\dagger\vec{\sigma}\vec{E}_p)/(\vec{E}_p^\dagger\vec{E}_p)$, where $\vec{\sigma}$ is the vector of Pauli matrices $\vec{\sigma} = (\sigma_1 \quad \sigma_2 \quad \sigma_3)$ with $\sigma_1 = \begin{bmatrix} 1 & 0 \\ 0 & -1 \end{bmatrix}$, $\sigma_2 = \begin{bmatrix} 0 & 1 \\ 1 & 0 \end{bmatrix}$, and $\sigma_3 = \begin{bmatrix} 0 & -j \\ j & 0 \end{bmatrix}$, the vector propagation equations of SBS can be derived from (1) [see Appendix A1]:

$$\frac{dI_p}{dz} = \frac{r_0}{1+\xi^2}(1 + \hat{s}\cdot\hat{p})I_s I_p \tag{2-1}$$

$$\frac{dI_s}{dz} = \frac{r_0}{1+\xi^2}(1 + \hat{s}\cdot\hat{p})I_s I_p \tag{2-2}$$

$$\frac{d\hat{p}}{dz} = \vec{\beta}_p \times \hat{p} + \frac{r_0 I_s}{1+\xi^2}[\hat{s} - (\hat{s}\cdot\hat{p})\hat{p}] + \frac{r_0\xi}{1+\xi^2}I_s(\hat{p}\times\hat{s}) \tag{2-3}$$

$$\frac{d\hat{s}}{dz} = \vec{\beta}_s \times \hat{s} + \frac{r_0 I_p}{1+\xi^2}[\hat{p} - (\hat{s}\cdot\hat{p})\hat{s}] + \frac{r_0\xi}{1+\xi^2}I_p(\hat{s}\times\hat{p}) \tag{2-4}$$

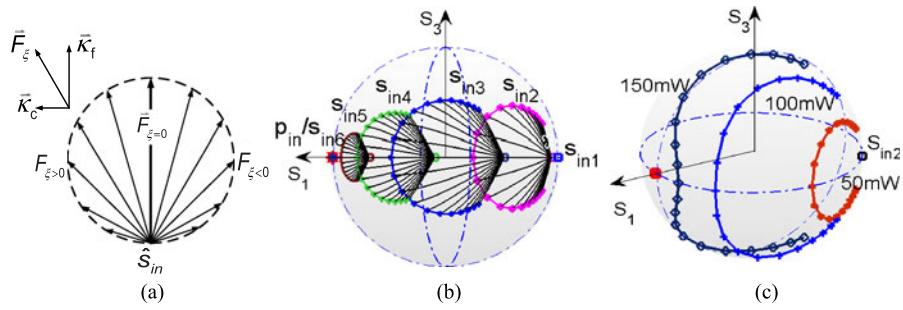

Fig. 2. (a) Schematic diagram of SBS pulling forces at $z = 0$. (b) Simulated spreadings for different $\hat{s}_{in}$s with $I_{p0} = 50$ mW. (c) Simulated spreadings for $\hat{s}_{in2}$ with different pump powers. Simulations are conducted with a 100 m SMF at $\hat{p}_{in} = (1, 0, 0)$ and $I_{s0} = 0.5$ mW.

where $r_0 = \omega_p^2 \gamma_e^2/(2\pi A_{\text{eff}} n c^3 \rho_0 v_A \Gamma_B)$ is the gain coefficient under the reasonable approximation of $\omega_p \approx \omega_s$ in SBS. A_{eff} is the effective area of fiber. $\xi = 2(\nu - \nu_B)/\Gamma_B$ refers to the normalized frequency detuning from ν_B. $\vec{\beta}_s = (\beta_1, \beta_2, \beta_3)$ and $\vec{\beta}_p = (-\beta_1, -\beta_2, \beta_3)$ denotes the polarization vectors of fiber for signal and pump lights. $\vec{\beta}_s$ consists of the linear birefringence $\vec{\beta}_l = (\beta_1, \beta_2, 0)$ and the circular birefringence $\vec{\beta}_c = (0, 0, \beta_3)$. It relates to $\mathbf{T}(z)$ by the following equation [6], [10]:

$$-2j\frac{dT}{dz}T^\dagger = \vec{\beta}_s \cdot \vec{\sigma}. \tag{3}$$

Equations (2-1) and (2-2) describe the power propagations of pump and signal. Equations (2-3) and (2-4) describe the polarization evolutions of pump and signal, in which the first terms represent the SOP evolution caused by fiber birefringence, and the second and the third terms represent the SBS induced nonlinear SOP evolution.

In depletion-free regime ($I_s \ll I_p$), the SBS pulling on $\hat{p}$ is negligible, whereas the SOP of ξ-component signal light, $\hat{s}_\xi$, experiences both the forward SBS pulling force $\vec{\kappa}_f$ in the direction of $\hat{p} - (\hat{s}_\xi \cdot \hat{p})\hat{s}_\xi = \hat{s}_\xi \times \hat{p} \times \hat{s}_\xi$, and the cross SBS pulling force $\vec{\kappa}_c$ in the direction of $\hat{s}_\xi \times \hat{p}$ with magnitudes

$$\begin{aligned} \|\vec{\kappa}_f\| &= \kappa_\xi \sqrt{1 - (\hat{s}_\xi \cdot \hat{p})^2} \\ \|\vec{\kappa}_c\| &= |\xi|\, \kappa_\xi \sqrt{1 - (\hat{s}_\xi \cdot \hat{p})^2} \end{aligned} \tag{4}$$

where $\kappa_\xi = r_0 I_p/(1 + \xi^2)$. The synthesized SBS pulling forces $\vec{F}_\xi$ are illustrated by arrowed lines in Fig. 2(a). It is seen that $\xi = 0$ component only experiences forward pulling, and $\xi \neq 0$ component experiences both. The cross forces on $\xi > 0$ and $\xi < 0$ components are in the opposite direction.

From Eq. (2-1)–(2-4), we have

$$\frac{d(\hat{s}_\xi \cdot \hat{p})}{dz} = 2\vec{\beta}_l \cdot (\hat{s}_\xi \times \hat{p}) + \kappa_\xi \left[1 - (\hat{s}_\xi \cdot \hat{p})^2\right] \tag{5}$$

and the SBS gain in depletion-free regime

$$G(\xi) = e^{\kappa_\xi L + \kappa_\xi \int_0^L (\hat{s}_\xi \cdot \hat{p})\, dz}. \tag{6}$$

Next, the SBS polarization spreadings in birefringence-free SMF, practical SMF, and PMF will be discussed separately. In addition, the spreading induced depolarization to a broadband light will be briefly discussed after that.

2.1. In Birefringence-Free SMFs

In the absence of fiber birefringence, (5) turns to be

$$\frac{d(\hat{s}_\xi \cdot \hat{p})}{dz} = \kappa_\xi \left[1 - (\hat{s}_\xi \cdot \hat{p})^2\right] \tag{7}$$

with solution in depletion-free regime [see Appendix A2]:

$$\hat{s}_\xi \cdot \hat{p} = \frac{Ce^{2\kappa_\xi L} - 1}{Ce^{2\kappa_\xi L} + 1} \tag{8}$$

where $C = (1 + u_0)/(1 - u_0)$, and $u_0 = \hat{s}_{\text{in}} \cdot \hat{p}_{z=0} = \hat{s}_{\text{in}} \cdot \hat{p}_{\text{in}}$ is the boundary condition at $z = 0$. $\xi = 0$ component experiences the maximum and minimum SBS gains of $G_0^{\max} = e^{2r_0 I_{p0} L}$ and $G_0^{\min} = 1$ at $u_0 = \pm 1$, respectively. Thus, we have

$$u_{\xi=0,out} = \hat{s}_{\xi=0} \cdot \hat{p} = \frac{G_0^{\max}/G_0^{\min}(1 + u_0) - (1 - u_0)}{G_0^{\max}/G_0^{\min}(1 + u_0) + (1 - u_0)}. \tag{9}$$

Because $\hat{s}_{\xi=0}$ dominates the heading direction of spreading profile, it is reasonable to evaluate the polarization spreading size with $u_{\xi=0,out}$ in the depletion-free regime.

The SBS polarization spreadings in birefringence-free SMFs are simulated by using the collocation iteration method, in which each step is calculated with the 4th Runge-Kutta algorithm. In simulations, $r_0 = 0.2229[\text{W} \cdot \text{m}]^{-1}$ is calculated with $\lambda_p = 1.55\ \mu$m, $\gamma_e = 0.902$, $A_{\text{eff}} = 80\ \mu\text{m}^2$, $v_A = 6000$ m/s, $c = 3 \times 10^8$ m/s, $\Gamma_B = 20$ MHz, $\rho_0 = 2.21 \times 10^3$ kg/m^3, and $n = 1.5$. Fig. 2(b) illustrates spectral polarization spreadings on the Poincaré sphere from different $\hat{s}_{\text{in}}$s marked with squares on the equator. In simulation, ξ is scanned from -2 to 2 with step of 0.2, $L = 100$ m, $\hat{p}_{\text{in}}$ is set at H(1, 0, 0), and input pump and signal powers are $I_{p0} = 50$ mW and $I_{s0} = 0.5$ mW. When $\hat{s}_{in6} = \hat{p}_{\text{in}}$ or $\hat{s}_{in1} = -\hat{p}_{\text{in}}$, which corresponds to the maximum or minimum SBS gain, no spreading occurs. For the cases between the two extremes, four circle-like spreadings heading toward $\hat{p}_{\text{in}}$ are illustrated. The spreadings are symmetrical about $\xi = 0$. The evolution trajectories of $\hat{s}_\xi$s (black lines) start from each $\hat{s}_{\text{in}}$ and end straightforwardly on the corresponding spreading profile.

Fig. 2(c) shows the simulated spreadings from $\hat{s}_{in2}$ with different pump powers of $I_{p0} = 50$, 100, and 150 mW. The spreading size increases with the elevation of pump power, and shows an inward concave in the central spectrum region for the large pump power. It is because the pulling force of the central spectrum region decreases more than that of side regions as the spreading profile approaches to $\hat{p}_{\text{in}}$. When $\hat{s}_\xi$ is very close to $\hat{p}_{\text{in}}$, the pulling force decreases to zero.

2.2 In Practical SMFs

In practical SMFs, the fiber birefringence is randomly distributed along the fiber. Generally, $\hat{s}_\xi$ randomly evolves on the Poincaré sphere along the fiber. However, the output signal can also been expressed with an overall Jones matrix **H** and decomposed by SVD method as [6], [11]

$$\vec{E}_{s,out} = \mathbf{H}\vec{E}_{s,in} = \mathbf{U}\mathbf{D}\mathbf{V}^\dagger \vec{E}_{s,in}. \tag{10}$$

In this section, only $\xi = 0$ is considered for the same reason as in yielding (9). In (10), **U** and **V** are unitary matrices, and $\mathbf{D} = diag(\sqrt{G_0^{\max}}, \sqrt{G_0^{\min}})$ is a diagonal matrix. $G_0^{\max}$ and $G_0^{\min}$ are the maximum and minimum SBS gains of $\xi = 0$ signal and the eigenvalues of $\mathbf{H}^\dagger\mathbf{H}$. Therefore, there exist eigenbases with respect to **H**: $\{\hat{e}_{\text{in}}^{\max}, \hat{e}_{\text{in}}^{\min}\}$ and $\{\hat{e}_{\text{out}}^{\max}, \hat{e}_{\text{out}}^{\min}\}$, which satisfy $\mathbf{V}^\dagger \hat{e}_{\text{in}}^{\max} = \begin{bmatrix} 1 \\ 0 \end{bmatrix}$, $\mathbf{V}^\dagger \hat{e}_{\text{in}}^{\min} = \begin{bmatrix} 0 \\ 1 \end{bmatrix}$, $\mathbf{U}^\dagger \hat{e}_{\text{out}}^{\max} = \begin{bmatrix} 1 \\ 0 \end{bmatrix}$ and $\mathbf{U}^\dagger \hat{e}_{\text{out}}^{\min} = \begin{bmatrix} 0 \\ 1 \end{bmatrix}$. Thus, for an arbitrary input signal linearly polarized in $\{\hat{e}_{\text{in}}^{\max}, \hat{e}_{\text{in}}^{\min}\}$ base

$$\vec{E}_{s,in} = \alpha_0 \hat{e}_{\text{in}}^{\max} + \beta_0 \hat{e}_{\text{in}}^{\min} \tag{11}$$

where α_0 and β_0 are components in $\hat{e}_{s,in}^{max/min}$ axes, the output signal is

$$\vec{E}_{s,out} = \alpha_0\sqrt{G_0^{\max}}\mathbf{U}\begin{bmatrix}1\\0\end{bmatrix} + \beta_0\sqrt{G_0^{\min}}\mathbf{U}\begin{bmatrix}0\\1\end{bmatrix} = \alpha_0\sqrt{G_0^{\max}}\hat{e}_{\text{out}}^{\max} + \beta_0\sqrt{G_0^{\min}}\hat{e}_{\text{out}}^{\min} \tag{12}$$

Defining $\hat{s}_{\text{in}}^{max/min}$ and $\hat{s}_{\text{out}}^{max/min}$ as SOPs of $\hat{e}_{\text{in}}^{max/min}$ and $\hat{e}_{\text{out}}^{max/min}$, and defining $u_0 = \hat{s}_{\text{in}} \cdot \hat{s}_{\text{in}}^{\max} = (\alpha_0^2 - \beta_0^2)/(\alpha_0^2 + \beta_0^2)$, we yield from (12)

$$u_{\xi=0,out} = \hat{s}_{\xi=0,out} \cdot \hat{s}_{\text{out}}^{\max} = \frac{G_0^{\max}/G_0^{\min}(1+u_0) - (1-u_0)}{G_0^{\max}/G_0^{\min}(1+u_0) + (1-u_0)}. \tag{13}$$

Equation (13) has the same form as (9). It indicates that spreading size $u_{\xi=0,out}$ is determined by $G_0^{\max}/G_0^{\min}$ and u_0. It also implies that the output SOP of signal in $\{\hat{s}_{\text{out}}^{\max}, \hat{s}_{\text{out}}^{\min}\}$ base can be expressed by $\hat{s}_{\text{in}}$ in $\{\hat{s}_{\text{in}}^{\max}, \hat{s}_{\text{in}}^{\min}\}$ base. The base transform from $\{\hat{s}_{\text{in}}^{\max}, \hat{s}_{\text{in}}^{\min}\}$ to $\{\hat{s}_{\text{out}}^{\max}, \hat{s}_{\text{out}}^{\min}\}$ is only determined by the fiber birefringence

$$\hat{s}_{\xi=0,out}^{max/min} = \mathbf{M}_L\,\hat{s}_{\text{in}}^{max/min}. \tag{14}$$

$\mathbf{M}_L$ is the Mueller matrix corresponding to $\mathbf{T}(L)$. Therefore, from the overall prospective, the evolution of $\hat{s}$ can be thought as firstly linearly rotating by $\mathbf{M}_L$ from $\{\hat{s}_{\text{in}}^{\max}, \hat{s}_{\text{in}}^{\min}\}$ base to $\{\hat{s}_{\text{out}}^{\max}, \hat{s}_{\text{out}}^{\min}\}$ base, then spreading with heading direction toward $\hat{s}_{\text{out}}^{\max}$ by SBS pulling as it does in SBS-only case. This behavior is consistent with the polarization decomposition theory of [12].

In depletion-free regime

$$ln r_g = ln\frac{G_0^{\max}}{G_0^{\min}} = 2r_0 I_{p0}\int_0^L \hat{s}_{\text{in}}^{\max\mathrm{T}}\mathbf{M}_{\mathbf{T}}^T(z)\mathbf{M}_{\mathbf{T}^*}(z)\mathbf{M}_L^T\hat{p}_{\text{in}}\,dz \tag{15}$$

where $\mathbf{M}_T(z)$ and $\mathbf{M}_{T^*}(z)$ are the Mueller matrices of $\mathbf{T}(z)$ and $\mathbf{T}^*(z)$. By assuming $c_b = \int_0^L \hat{s}_{\text{in}}^{\max\mathrm{T}}\mathbf{M}_{\mathbf{T}}^T(z)\mathbf{M}_{\mathbf{T}^*}(z)\mathbf{M}_L^T\hat{p}_{\text{in}}\,dz/L$, and referring (7), (13) is the solution of

$$\frac{d(\hat{s}_{\xi=0}\cdot\hat{s}_{\text{out}}^{\max})}{dz} = r_0 I_{p0} c_b[1 - (\hat{s}_{\xi=0}\cdot\hat{s}_{\text{out}}^{\max})^2]. \tag{16}$$

Comparing (16) with the counterpart of SBS-only case, in practical SMFs, the equivalent SBS pulling force in $\{\hat{s}_{\text{out}}^{\max}, \hat{s}_{\text{out}}^{\min}\}$ base is dependent on the fiber birefringence and reduced by the factor of c_b.

Next, we will discuss the influence of birefringence randomness of fiber on SBS polarization spreading. Generally, both r_g and $\{\hat{s}_{\text{out}}^{\max}, \hat{s}_{\text{out}}^{\min}\}$ base are dependent on $\hat{p}_{\text{in}}$ and the fiber birefringence. In short SMF with less birefringence randomness, the traces of $\hat{s}$ and $\hat{p}$ along the fiber are not ergodic on Poincaré sphere. There exists $\hat{p}_{\text{in}}^{\max}$, resulting in the global maximum SBS gain and $r_g = r_{\text{gmax}}$. Thus, spreadings in $\{\hat{s}_{\text{out,global}}^{\max}, \hat{s}_{\text{out,global}}^{\min}\}$ base are of the maximum size. When $\hat{p}_{\text{in}} \neq \hat{p}_{\text{in}}^{\max}$, $r_g < r_{\text{gmax}}$, and spreading size is smaller.

In long fiber with full birefringence randomness, where fiber length much larger than the beat length and the birefringence correlation length, the SOP trace is ergodic. For arbitrary $\hat{p}_{\text{in}}$, there always exists $\hat{s}_{\text{out}}^{\max} = \mathbf{M}\hat{p}_{\text{in}}$, in which $\mathbf{M} = diag(1, 1, -1)$ [7], [13], [14]. Thus, we have $c_b = 1/3$, and $ln r_g = 2/3 r_0 I_{p0} L$. Therefore in a long SMF, the spreading size is independent of $\hat{p}_{\text{in}}$ and one third of that in SBS-only fiber.

Fig. 3 shows the simulations for a 100 m SMF with less birefringence randomness. The simulation steps are as follows. First, one random birefringence realization with average beat length of 20 m and birefringence correlation length of 10 m is generated. Second, 10000 times of simulation with (2-1) and (2-4) are conducted with the free combinations of 100−spherical-uniformly distributed $\hat{p}_{\text{in}}$s and the same 100 $\hat{s}_{\text{in}}$s, in order to search for $\{\hat{s}_{\text{in}}^{\max}, \hat{s}_{\text{in}}^{\min}\}$, $\{\hat{s}_{\text{out}}^{\max}, \hat{s}_{\text{out}}^{\min}\}$ and r_g for each $\hat{p}_{\text{in}}$. Fig. 3(a) shows the simulation for the global maximum gain case among the 100 $\hat{p}_{\text{in}}$s. $\{\hat{s}_{\text{in,global}}^{\max}, \hat{s}_{\text{in,global}}^{\min}\}$ (red diamond and circle), $\hat{p}_{\text{in}}^{\max}$ (blue square), and $\{\hat{s}_{\text{out,global}}^{\max}, \hat{s}_{\text{out,global}}^{\min}\}$ are indicated. 9 $\hat{s}_{\text{in}}$s ($\hat{s}_{\text{in,global}}^{\max}$, $\hat{s}_{in2} - \hat{s}_{in8}$, $\hat{s}_{\text{in,global}}^{\min}$) are chosen in an orthodrome crossing $\hat{s}_{\text{in,global}}^{\max}$ with $\pi/8$ angle space. The simulated spreadings head toward $\hat{s}_{\text{out,global}}^{\max}$ orderly in the same way as in the SBS-only case. No spreadings

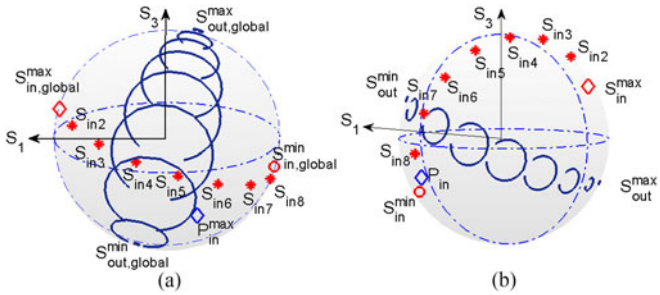

Fig. 3. Simulated spreadings for a 100 m SMF with a birefringence realization of average beat length of 20 m and birefringence correlation of 10 m. (a) $\hat{p}_{\text{in}} = \hat{p}_{\text{in}}^{\max}$ with $r_{\text{gmax}} = 5.1563$. (b) $\hat{p}_{\text{in}} \neq \hat{p}_{\text{in}}^{\max}$ with $r_g = 1.99$.

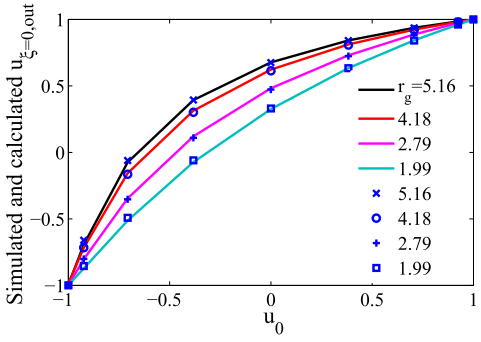

Fig. 4. Relationships between $u_{\xi=0,out}$ and u_0 for different r_gs by simulations of (2-1)–(2-4) (solid lines) and calculation of (12) (blue markers).

occurs at $\hat{s}_{\text{in,global}}^{\max}$ and $\hat{s}_{\text{in,global}}^{\min}$. $r_{\text{gmax}} = 5.1563$ for the birefringence realization. Fig. 3(b) shows the spreadings for a $\hat{p}_{\text{in}} \neq \hat{p}_{\text{in}}^{\max}$ case, where $r_g = 1.99$, which is the smallest one among all simulated $\hat{p}_{\text{in}}$s. $\{\hat{s}_{\text{in}}^{\max}, \hat{s}_{\text{in}}^{\min}\}$ is shown with red diamond and circle. The spreadings head to $\hat{s}_{\text{out}}^{\max}$ in the same way as those in $\hat{p}_{\text{in}}^{\max}$-case, but with smaller sizes. Fig. 4 gives the simulated relations between $u_{\xi=0,out}$ and $u_0 = \hat{s}_{\text{in}} \cdot \hat{s}_{\text{in}}^{\max}$ for $r_g = 5.16, 4.18, 2.79$, and 1.99, respectively. The calculation results of (13) are also given with blue markers in Fig. 4. Two results are well consistent. The tiny differences between the two results are due to the positioning uncertainty of $\hat{s}_{\text{in}}^{\max}$s, which are the ones mostly near the real $\hat{s}_{\text{in}}^{\max}$s among the 100 generated SOPs, rather than the real $\hat{s}_{\text{in}}^{\max}$s.

2.3 In PMFs

In PMFs, only fixed linear birefringence exists, and $\vec{\beta}_s = -\vec{\beta}_p = \vec{\beta}_l = 2\pi/L_b\hat{\beta}_l$, where L_b is the beat length of fiber. $\hat{\beta}_l$ is the unit vector of $\vec{\beta}_l$ and lies in the equatorial plane. Along z-direction, $\hat{s}_\xi$ and $\hat{p}$ rotate oppositely in two parallel circles perpendicular to $\vec{\beta}_l$ at the speed of $2\pi/L_b$ by the birefringence force. However, $\hat{s}_\xi$ simultaneously experiences the SBS pulling toward the local $\hat{p}$. We consider the evolution of $\xi = 0$ component for the same reason as in the discussion of SMFs. Locally within one $L_b/2$ period, SBS pulling force $\vec{F}_{\xi=0}$ changes direction alternately. However, the overall heading direction of the spreading profile is dominated by the average of $\vec{F}_{\xi=0}$. From (2-4), it is derived that

$$\begin{aligned}\frac{d\hat{s}_{\xi=0}}{dz} \cdot \hat{\beta}_l &= r_0 l_p \left[\hat{p} \cdot \hat{\beta}_l - (\hat{s}_{\xi=0} \cdot \hat{p})(\hat{s}_{\xi=0} \cdot \hat{\beta}_l)\right] \\ &= r_0 l_p \{\hat{p} \cdot \hat{\beta}_l - [(\hat{s}_{\xi=0} \times \hat{\beta}_l) \cdot (\hat{p} \times \hat{\beta}_l) + (\hat{s}_{\xi=0} \cdot \hat{\beta}_l)(\hat{p} \cdot \hat{\beta}_l)](\hat{s}_{\xi=0} \cdot \hat{\beta}_l)\} \\ &\approx r_0 l_{p0} \hat{p}_{\text{in}} \cdot \hat{\beta}_l \left[1 - (\hat{s}_{\xi=0} \cdot \hat{\beta}_l)^2\right]. \end{aligned} \tag{17}$$

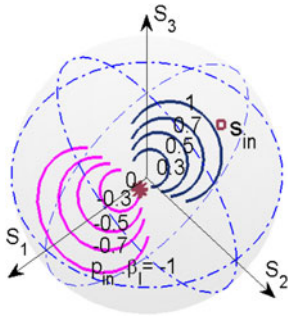

Fig. 5. Simulation polarization spreadings for different $\hat{p}_{\text{in}} \cdot \hat{\beta}_l$s in PMF. In simulation $L = 100$ m, $L_b = 10$ m, $\hat{\beta}_l = (-1, 0, 0)$, $I_{s0} = 0.5$ mW, and $I_{p0} = 50$ mW.

Equation (17) is obtained with the reasonable approximation that the average effect of $(\hat{s}_{\xi=0} \times \hat{\beta}_l) \cdot (\hat{p} \times \hat{\beta}_l)(\hat{s}_{\xi=0} \cdot \hat{\beta}_l)$ over a period of $L_b/2$ is zero. Equation (17) indicates that in PMFs for an arbitrary $\hat{p}_{\text{in}}$, $\hat{s}_{\text{in}}^{\max} = \hat{s}_{\text{out}}^{\max} = sign(\hat{p}_{\text{in}} \cdot \hat{\beta}_l)\hat{\beta}_l$ and $c_b = |\hat{p}_{\text{in}} \cdot \hat{\beta}_l|$, i.e., spreadings always head toward $sign(\hat{p}_{\text{in}} \cdot \hat{\beta}_l)\hat{\beta}_l$ with $c_b = |\hat{p}_{\text{in}} \cdot \hat{\beta}_l|$.

Given a 100 m PMF with $L_b = 10$ m, $\hat{\beta}_l = (-1, 0, 0)$, $I_{s0} = 0.5$ mW, and $I_{p0} = 50$ mW, Fig. 5 shows the spreadings for $\hat{p}_{\text{in}} \cdot \hat{\beta}_l = 1, \pm 0.7, \pm 0.5, \pm 0.3, 0$ from the given $\hat{s}_{\text{in}}$ (marked with square). It is shown that when $\hat{p}_{\text{in}} \cdot \hat{\beta}_l$ changes the sign, the spreading orientation switches to the opposite. Spreading sizes reach their largest amounts as $|\hat{p}_{\text{in}} \cdot \hat{\beta}_l| = 1$, and decrease as $|\hat{p}_{\text{in}} \cdot \hat{\beta}_l|$ decreases. When $\hat{p}_{\text{in}} \cdot \hat{\beta}_l = 0$, no spreading occurs, as shown by the point in the middle of spreading curves in Fig. 5.

2.4 Spreading Induced Depolarization

Because the light frequency within the SBS bandwidth experiences polarization spreading, a broadband signal will suffer depolarization. The DOP of output signal can be expressed as

$$DOP = \frac{I_{\max} - I_{\min}}{I_{\max} + I_{\min}} = \frac{\int G(\xi)\alpha(\xi)d\xi - \int G(\xi)(1-\alpha(\xi))d\xi}{\int G(\xi)d\xi} \tag{18}$$

where $I_{\max}$ and $I_{\min}$ are the maximum and minimum powers accumulated in the two orthogonal vectors $\pm\hat{r}_{\max}$. $G(\xi)\alpha(\xi)$ and $G(\xi)(1-\alpha(\xi))$ are the powers of ξ-component decomposed in $\pm\hat{r}_{\max}$. Geometrically, we have $\alpha(\xi) = (1 + \hat{s}_\xi \cdot \hat{r}_{\max})/2$, which implies the influence of polarization spreading on DOP. From Eq.(18), DOP is the function of SBS gain, signal bandwidth, and the polarization spreading. Generally, for signal with bandwidth less than SBS bandwidth $\hat{r}_{\max} \approx \hat{s}_{\xi=0,out}$.

3 Experimental Results

The experimental setup to observe the SBS polarization spreading is illustrated in Fig. 6. A light of 1553 nm from Santec ECL200 with linewidth of 0.2 MHz is employed. Through a 1:1 coupler, one beam, used as signal light, is modulated with a sweeping radio frequency electrical signal (RF) from 10730 MHz to 10830 MHz through an electro-optical modulator (EOM). The $v + v_B$ light is filtered out through a fiber Bragg grating (FBG), and the $v - v_B$ light is launched into the fiber through circulator1. The other beam, used as pump light, is amplified by an Erbium doped optical fiber amplifier (EDFA) and launched into the other end of the fiber through circulator2. Four polarization controllers (PCs) are used: PC1 for the polarization alignment to EOM, PC2 for adjusting the input SOPs of pump, PC3 cascaded with a polarizer (P), a half-wave plate (HWP) and PC4 is used for adjusting the input SOP of signal and choosing $\hat{s}_{\text{in}}$s in an orthodrome of $\{\hat{s}_{\text{in}}^{\max}, \hat{s}_{\text{in}}^{\min}\}$ base. The output SOP and power of signal light are measured simultaneously by a polarization state analyzer (PSA).

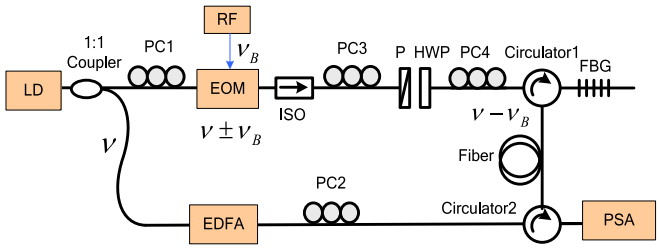

Fig. 6. Experimental setup, in which PC: polarization controller; P: polarizer; HWP: half-wave plate; FBG: fiber Bragg grating; EDFA: Erbium-doped fiber amplifier; ISO: isolator; EOM: electro-optical modulator; and PSA: polarization state analyzer.

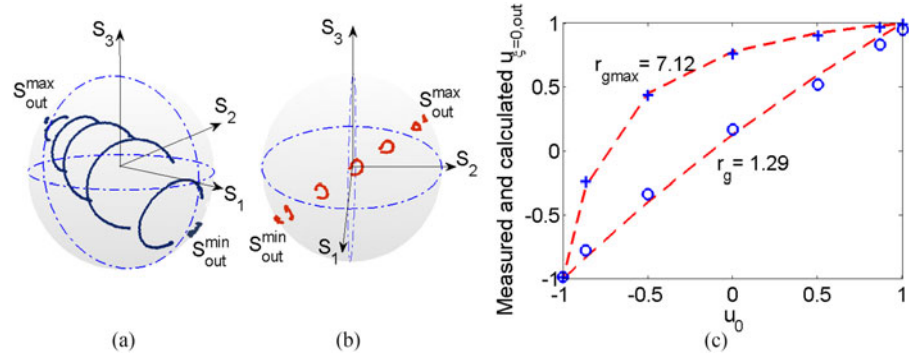

Fig. 7. Measured spreadings in the cases of (a) $\hat{p}_{\text{in}} = \hat{p}_{\text{in}}^{\max}$ with measured $r_{\text{gmax}} = 7.12$ and (b) $\hat{p}_{\text{in}} \neq \hat{p}_{\text{in}}^{\max}$ with measured $r_g = 1.29$ for 7 chosen $\hat{s}_{\text{in}}$s. (c) Measured (blue markers) and the calculated (red dash lines) relationships between $u_{\xi=0,out}$ and u_0 for the two $\hat{p}_{\text{in}}$ cases. In measurement $I_{p0} = 63$ mW, $I_{s0} = 0.5$ mW, and $L = 200$ m.

In experiment, a 200 m SMF and a small signal power $I_{s0} = 0.5$ mW are used for avoiding pump depletion. The polarization spreadings corresponding to 7-$\hat{s}_{\text{in}}$, which are obtained by rotating the HWP through a $\pi/24$-angle each time, are measured with pump powers of $I_{p0} = 63$ mW. Spreadings of two $\hat{p}_{\text{in}}$ cases are measured. Fig. 7(a) is for the case of $\hat{p}_{\text{in}} = \hat{p}_{\text{in}}^{\max}$, where $r_{\text{gmax}} = 7.12$ is measured. Fig. 7(b) is for the case of $\hat{p}_{\text{in}} \neq \hat{p}_{\text{in}}^{\max}$ with $r_g = 1.29$, which is the smallest measured value for the fiber. In each case, spreadings head toward an unique $\hat{s}_{\text{out}}^{\max}$, and perform consistently with the theoretical simulations in Fig. 3. In addition, fibers with different lengths are also measured. The $\hat{p}_{\text{in}}$ induced variation of r_g can be measured in a 2 km SMF, and disappears in a 5 km and other longer SMFs in our experiments. Fig. 7(c) presents the measured relationships between $u_{\xi=0,out}$ and u_0 (blue markers) for the two cases, and the calculated results (red dash lines) are also presented. Two results are consistent, although some errors occur in $r_g = 1.29$ case due to the difficulty in positioning $\hat{s}_{\text{in}}^{\max}$ in the small r_g case.

Theoretically, the spreading size increases with the increase of pump power. Fig. 8(a) shows the spreadings for different pump powers at $u_0 = -0.2588$. As spreading profile approaches to $\hat{s}_{\text{out}}^{\max}$ (red circle), the central region of the spreading profiles show flattened and a little bit inward concave. Fig. 8(b) shows the measured relationships between $u_{\xi=0,out}$ and the pump power for different u_0s, and the calculated results with (13) are also presented with red dashed lines. Two results are in good agreement. In calculation, the relation $r_g = r_{g1}^{I_{p0}/I_{p01}}$ derived from (15) is used. This indicates that by just measuring r_{g1} of pump power I_{p01}, the r_gs at the other I_{p0}s can be evaluated.

Moreover, the orientation switching of polarization spreading in PMF is measured with a 140 m PMF at $I_{p0} = 47$ mW, as shown in Fig. 9. In experiment, the spreading profiles are measured by fixing $\hat{s}_{\text{in}}$ and randomly adjusting $\hat{p}_{\text{in}}$. It is seen that the orientation of spreading switches between two opposite directions for arbitrary $\hat{p}_{\text{in}}$s. This behavior is well consistent with the simulations in Fig. 5.

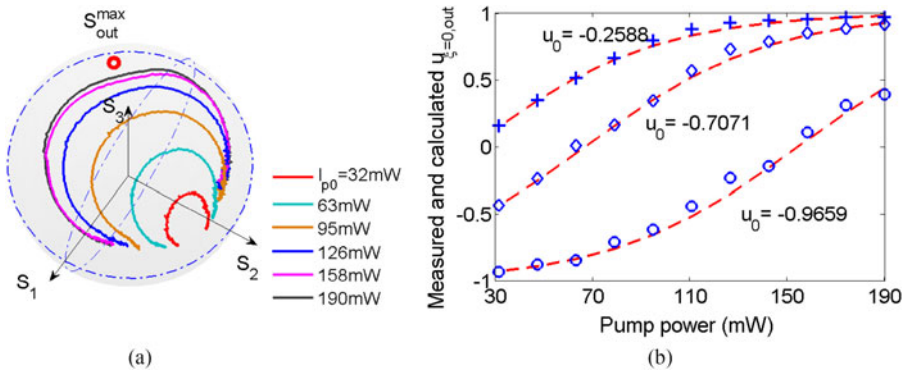

Fig. 8. (a) Measured spreadings in the 200 m fiber for different pump powers at $u_0 = -0.2588$. (b) Measured (blue markers) and calculated (red dash lines) relationships between $u_{\xi=0,out}$ and the pump power for different u_0s.

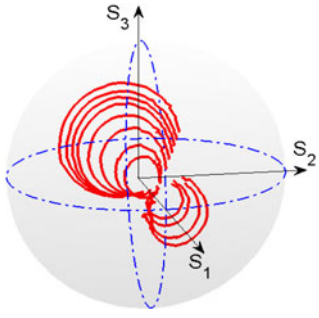

Fig. 9. Measured spreadings in a 140 m PMF for a fixed $\hat{s}_{\text{in}}$ with randomly adjusted $\hat{p}_{\text{in}}$s. In experiment, $I_{p0} = 47$ mW and $I_{s0} = 0.5$ mW.

4 Conclusion

From the proposed spectral vector model, the spectral polarization spreading phenomenon in SBS is revealed. The polarization behaviors in birefringence-free SMF, practical SMF, and PMF are thoroughly investigated by analytical discussion, simulation and experiment. In arbitrary fiber with a given input SOP of pump light, the SBS polarization spreading concurring with fiber birefringence effect can be thought as the linear-rotation by the fiber birefringence followed with the SBS spreading heading towards $\hat{s}_{\text{out}}^{\max}$, which refers to the output SOP of the signal light that experiences the largest SBS gain. The spreading size is decided directly by the ratio of the maximum to minimum SBS gain and the projection of input SOP of signal on $\hat{s}_{\text{in}}^{\max}$. Both parameters are functions of fiber birefringence and input SOP of pump. Especially in PMFs, because $\hat{s}_{\text{out}}^{\max}$ is parallel with the fix polarization vector, an orientation switching performance of the polarization spreading is observed. Finally, the SBS polarization spreadings are demonstrated with a 200 m SMF and a 140 m PMF experimentally. The experimental observations and measurements of polarization spreadings are consistent with the theoretical results.

Based on the revealed SBS polarization spreading, some potential applications can be expected by taking the advantage of the polarization distinction, such as polarization mode-locking, polarization dependent filter, polarization switching. For instance, by the polarization spreading theory, we have made a reasonable explanation to a polarization dependent deviation of SBS frequency shift, which was experimentally observed in BOTDA by Xie *et al.* [15], but remained the mechanism unclear. It is actually caused by the fiber birefringence induced twist on the spreading profile. This work will be addressed in another paper.

Appendix A1

Equations (2-1) and (2-2) are the same as the intensity evolution equations given in [6]. The derivation of (2-4) is as follows:

$$\frac{d\hat{s}}{dz} = \frac{d}{dz}\left(\frac{\vec{E}_s^{\dagger}\vec{\sigma}\vec{E}_s}{\vec{E}_s^{\dagger}\vec{E}_s}\right) = \frac{1}{I_s}\frac{d(\vec{E}_s^{\dagger}\vec{\sigma}\vec{E}_s)}{dz} - \frac{r_0}{1+\xi^2}\hat{s}(1+\hat{s}\cdot\hat{p})I_p. \tag{A1-1}$$

According to [10]

$$\begin{aligned}
\frac{d(\vec{E}_s^{\dagger}\vec{\sigma}\vec{E}_s)}{dz} &= \frac{d\vec{E}_s^{\dagger}}{dz}\vec{\sigma}\vec{E}_s + \vec{E}_s^{\dagger}\vec{\sigma}\frac{d\vec{E}_s}{dz} \\
&= \vec{E}_s^{\dagger}\left(T(z)\frac{dT^{\dagger}(z)}{dz} + \frac{r_0}{1+j\xi}(\vec{E}_p\vec{E}_p^{\dagger})\right)\vec{\sigma}\vec{E}_s + \vec{E}_s^{\dagger}\vec{\sigma}\left(\frac{dT(z)}{dz}T^{\dagger}(z) + \frac{r_0}{1-j\xi}(\vec{E}_p\vec{E}_p^{\dagger})\right)\vec{E}_s \\
&= \vec{E}_s^{\dagger}\left(-\frac{j}{2}\vec{\beta}\cdot\vec{\sigma} + \frac{r_0 I_p}{2(1+j\xi)}(\mathbf{I}_{3\times3} + \hat{p}\cdot\vec{\sigma})\right)\vec{\sigma}\vec{E}_s \\
&\quad + \vec{E}_s^{\dagger}\vec{\sigma}\left(\frac{j}{2}\vec{\beta}\cdot\vec{\sigma} + \frac{r_0 I_p}{2(1-j\xi)}(\mathbf{I}_{3\times3} + \hat{p}\cdot\vec{\sigma})\right)\vec{E}_s \\
&= \vec{\beta}\times\hat{s}I_s + \frac{r_0 I_p}{2(1+\xi^2)}\left[2\hat{s}I_s + 2\vec{E}_s^{\dagger}(\hat{p}\mathbf{I}_{3\times3})\vec{E}_s\right] + \frac{r_0\xi I_p}{2(1+\xi^2)}\left[2\vec{E}_s^{\dagger}(\hat{p}\times\vec{\sigma})\vec{E}_s\right] \\
&= \vec{\beta}\times\hat{s}I_s + \frac{r_0 I_s I_p}{1+\xi^2}(\hat{p}+\hat{s}) + \frac{r_0\xi I_s I_p}{1+\xi^2}\hat{p}\times\hat{s}.
\end{aligned} \tag{A1-2}$$

$\mathbf{I}_{3\times3}$ is a 3×3 unit matrix. If we substitute (A1-2) into (A1-1), we can obtain (2-4), and (2-3) can be derived similarly.

Appendix A2

Assuming $\hat{s}_\xi\cdot\hat{p} = u$, (5) becomes

$$\frac{du}{dz} = \kappa_\xi(1-u^2) \tag{A2-1}$$

with boundary condition $u_0 = \hat{s}_{\text{in}}\cdot\hat{p}_{\text{in}}$. Because

$$\int\frac{du}{\kappa_\xi(1-u^2)} = \frac{1}{2\kappa_\xi}\left(\int\frac{du}{1-u} + \int\frac{du}{1+u}\right) = \frac{1}{2\kappa_\xi}ln\frac{1+u}{1-u} \tag{A2-2}$$

the solution can be derived as

$$\hat{s}_\xi\cdot\hat{p} = \frac{Ce^{2\kappa_\xi L}-1}{Ce^{2\kappa_\xi L}+1} \tag{A2-3}$$

where $C = (1+u_0)/(1-u_0)$.

References

[1] X. Bao and L. Chen, "Recent progress in optical fiber sensors based on Brillouin scattering at University of Ottawa," *Photon. Sensors*, vol. 1, pp. 102–117, 2011.

[2] O. Terra, G. Groshe, and H. Schnatz, "Brillouin amplification in phase coherent transfer of optical frequencies over 480 km fiber," *Opt. Exp.*, vol. 18, pp. 16102–16111, 2010.

[3] J. C. Yong, L. Thévenaz, and B. Y. Kim, "Brillouin fiber laser pumped by a DFB laser diode," *J. Lightw. Technol.*, vol. 21, no. 2, pp. 546–555, Feb. 2003.

[4] L. Thévenaz, A. Zadok, A. Eyal, and M. Tur, "All-optical polarization control through Brillouin amplification," in *Proc. Conf. Opt. Fiber Commun.*, 2008, Paper OML7.

[5] A. Zadok, E. Zilka, A. Eyal, L. Thévenaz, and M. Tur, "Fiber beat length estimates via polarization measurements of stimulated Brillouin scattering amplified signals," in *Proc. Conf. Opt. Fiber Commun.*, 2009, Paper OMP4.

[6] A. Zadok, E. Zilka, A. Eyal, L. Thévenaz, and M. Tur, "Vector analysis of stimulated Brillouin scattering amplification in standard single-mode fibers," *Opt. Exp.*, vol. 16, pp. 21692–21707, 2008.
[7] O. Shlomovits and M. Tur, "Vector analysis of depleted stimulated Brillouin scattering amplification in standard single-mode fibers with nonzero birefringence," *Opt. Lett.*, vol. 38, pp. 836–838, 2013.
[8] J. Fatome, S. Pitois, and G. Millot, "Experimental evidence of Brillouin-induced polarization wheeling in highly birefringent optical," *Opt. Exp.*, vol. 17, pp. 12612–12618, 2009.
[9] R. W. Boyd, *Nonlinear Optics.* New York, NY, USA: Academic, 2003, ch. 9, pp. 409–427.
[10] J. P. Gordon and H. Kogelnik, "PMD fundamentals: Polarization mode dispersion in optical fibers," *Proc. Nat. Acad. Sci. USA*, vol. 97, no. 9, pp. 4541–4550, 2000.
[11] S.-Y. Lu and R. A. Chipman, "Interpretation of Mueller matrices based on polar decomposition," *J. Opt. Soc. Amer. A*, vol. 13, pp. 1106–1113, 1996.
[12] S.-Y. Lu and R. A. Chipman, "Homogeneous and inhomogeneous Jones matrices," *J. Opt. Soc. Amer. A*, vol. 11, 1994, Art. no. 766C773.
[13] M. O. Van Deventer and A. J. Boot, "Polarization properties of stimulated Brillouin scattering in single-mode fibers," *J. Lightw. Technol.*, vol. 12, no. 4, pp. 585–590, Apr. 1994.
[14] L. Ursini, M. Santagiustina, and L. Palmieri, "Polarization-dependent Brillouin gain in randomly birefringent fiber," *IEEE Photon. Technol. Lett.*, vol. 22, no. 10, pp. 712–714, May 2010.
[15] S. Xie, M. Peng, X. Bao, and L. Chen, "Polarization dependence of Brillouin linewidth and peak frequency due to fiber inhomogeneity in signal mode fiber and its impact on distributed fiber Brillouin sensing," *Opt. Exp.*, vol. 20, pp. 6385–6399, 2012.